ELSEVIER

High strength ductile Cu-base metallic glass

J. Eckert [a,*], J. Das [a,b], K.B. Kim [a,c], F. Baier [a],
M.B. Tang [d], W.H. Wang [d], Z.F. Zhang [e]

[a] FG Physikalische Metallkunde, FB 11 Material- und Geowissenschaften,
Technische Universität Darmstadt, Petersenstraße 23, D-64287 Darmstadt, Germany
[b] IFW Dresden, Institut für Metallische Werkstoffe, Postfach 270016, D-01171 Dresden, Germany
[c] Department of Advanced Materials Engineering, Sejong University, 98 Gunja-dong, Gwangjin-gu, Seoul, 143-747, Korea
[d] Institute of Physics, Chinese Academy of Sciences, Beijing 100080, China
[e] Shenyang National Laboratory for Materials Science, Institute of Metal Research,
Chinese Academy of Sciences, 72 Wenhua Road, Shenyang 110016, China

Abstract

Usually, bulk metallic glasses exhibit strength values superior to conventional crystalline alloys, often combined with a large elastic limit and rather low Young's modulus. This combination of properties renders such alloys quite unique when compared to commercial materials. However, the major drawback for engineering applications is their limited room temperature ductility and toughness due to the localized deformation processes linked to shear banding, where high plastic deformation is accumulated in a very narrow region without contributing to macroscopic deformation, work hardening or yielding. In this work we report on a new class of metallic glass in a simple Cu-base alloy. Addition of 5 at.% Al increases the glass-forming ability of binary $Cu_{50}Zr_{50}$. The resulting $Cu_{47.5}Zr_{47.5}Al_5$ glass exhibits high strength (2265 MPa) together with large room temperature ductility up to 18%. After yielding a strong increase in the flow stress is observed during deformation. The structure of the metallic glass exhibits atomic-scale heterogeneities that enable easy nucleation and continuous multiplication of shear bands. The interaction and intersection of shear bands increases the flow stress of the material with further deformation, leading to a 'work hardening'-like behavior and yields a continuous rotation of the shear angle up to fracture resulting in a high compressive ductility.
© 2006 Elsevier Ltd. All rights reserved.

Keywords: B. Glasses, metallic; B. Mechanical properties at ambient temperature; B. Work-hardening; D. Microstructure

1. Introduction

The recent finding of bulk glass formation in simple binary alloys [1–4] has received a lot of attention and is promising for the further development of bulk metallic glasses (BMGs) with potential for technological applications. Among these alloys, a series of binary Cu-base glasses has been reported [1,3–5]. A high glass-forming ability has also been reported for Cu-base ternary Cu–Zr–Al [6] and quaternary $Cu_{46}Zr_{47-x}Al_7Y_x$ [7] alloys that have been derived from the binary glass-forming compositions.

Generally, bulk metallic glasses show a macroscopically rather brittle deformation behavior at room temperature and exhibit near theoretical strength before failure due to the absence of dislocation-based plasticity [8]. The limited macroscopic plastic deformability of BMGs is correlated with highly localized deformation processes [9], such as shear banding, where a high amount of plastic strain is accumulated in a very narrow region exhibiting strain softening/thermal softening [10]. Failure finally occurs along a dominant single shear band [11] with typically less than 1% plastic strain.

In the past decades, continuous attempts have been made in order to enhance the ductility of multicomponent bulk metallic glasses through designing a composite microstructure. In this context, the first attempt was to improve the strength and ductility by introducing nanocrystalline [12,13] or nano-quasicrystalline [14–16] precipitates in a glassy matrix after partial crystallization by controlled annealing treatment of amorphous precursors. In addition, composites containing

* Corresponding author. Address: FG Physikalische Metallkunde, FB 11 Material- und Geowissenschaften, Technische Universität Darmstadt, Petersenstraße 23, D-64287 Darmstadt, Germany. Tel.: +49 6151 162946; fax: +49 6151 165557.
E-mail address: j.eckert@phm.tu-darmstadt.de (J. Eckert).

micrometer-size ductile phases are suitable to enhance the ductility of monolithic BMGs [17]. These glass-matrix based composites can be classified in two groups according to the way they are processed: (i) ex situ and (ii) in situ formed composites. The ex situ composites are obtained by introducing a crystalline solid phase as reinforcement into the glass-forming melt during solidification and contain either particle reinforcements [17–19] or fiber reinforcements [20–23] (continuous or discontinuous fibers). The in situ composites are formed from their melts directly during solidification, containing either nano/micrometer-size particles, [12,24,25] or ductile dendrites in a residual glassy matrix [26,27]. Especially the in situ ductile dendritic phase reinforced composites have been found to be successful in combating catastrophic shear banding, whereby the room temperature ductility of BMGs is increased significantly. Taking advantage of this successful approach, a similar composite microstructure has been produced by casting in Zr- [28–30] and Ti-base [31,32] alloy systems, where a high strength nanostructured matrix is combined with a ductile dendritic solid solution as toughening phase.

A significant ductility was also observed recently in monolithic quinary Zr–Ti/Ta–Cu–Ni–Al (plastic strain, $\varepsilon_p = 4.5\%$) [33], and quaternary Pt–Cu–Ni–P ($\varepsilon_p = 20\%$) [34] BMGs. The ductility of these metallic glasses has been correlated [34] with their elastic properties (low shear/bulk modulus ratio and high Poisson's ratio) allowing for a shear collapse and an extension of the tip of a shear band thus controlling the extension instability of crack nucleation. Very recent work [35] on the development of ductile bulk metallic glasses has shown a significant increase in the flow stress during deformation, similar as it is well known for crystalline metals and alloys.

In this article, we present a new class of inherently ductile bulk metallic glass. This novel Cu-base BMG is rather simple and cheap to produce, and exhibits an exceptional combination of high strength (2265 MPa) with a plastic deformation up to 18% strain. The unique structural backbone of this glassy material significantly enhances the easy nucleation of shear bands, their wavy movement and continuous branching. Finally, the correlation between the rotation of the shear plane with the high compressive plasticity of the BMGs will be described.

2. Experimental

The binary $Cu_{50}Zr_{50}$ and ternary $Cu_{47.5}Zr_{47.5}Al_5$ alloys were prepared by arc melting of the pure elements under an argon atmosphere with appropriate portions of Zr, Cu, and Al to obtain the desired alloy composition. The alloys were remelted several times in order to achieve homogeneity and finally 2 mm diameter cylindrical rods were prepared in an in situ suction casting facility attached to the arc-melter.

Structural investigations were carried out by X-ray diffraction (XRD) with Cu K_α radiation using a Siemens D500 diffractometer. Thin slices from the as-cast rods were prepared by the conventional method of slicing and grinding, followed by dimpling and finally ion-milling (BAL-TEC RES 010). These slices were used for detailed structural investigations of the as-cast samples by high-resolution transmission electron microscopy (HR-TEM, Philips CM 20) coupled with energy-dispersive X-ray analysis (EDX, Noran). The thermal stability of the as-cast alloys was examined with a differential scanning calorimeter (Perkin Elmer Dimond DSC) under a flow of purified argon using a constant heating rate of 40 K/min.

In order to evaluate the mechanical properties under compression, cylindrical specimens of 2 mm diameter and 4 mm length were prepared from the as-cast rods and tested in a Schenck hydraulic testing machine under quasistatic loading at an initial strain rate of $8 \times 10^{-4}\,s^{-1}$ at room temperature. Both ends of the specimens were polished to make them parallel to each other prior to the compression test. The strain in the sample was measured from the displacement of the machine cross heads. Before performing the test, the machine was calibrated. At first, a load–displacement curve for the machine was obtained without any specimen up to 30 kN. This load–displacement data was subtracted from those of the tests with the samples to estimate the actual strain under dynamic
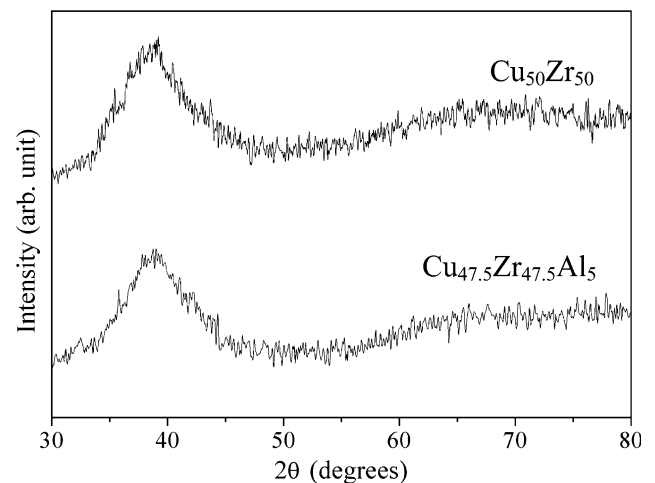

Fig. 1. X-ray diffraction patterns (Cu K_α radiation) for (a) $Cu_{50}Zr_{50}$ and (b) $Cu_{47.5}Zr_{47.5}Al_5$. The broad diffuse diffraction maxima reveal the amorphous nature of the alloys.
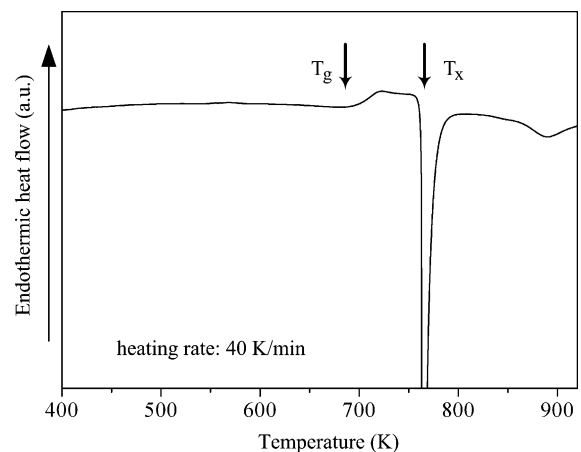

Fig. 2. DSC trace (heating rate 40 K/min) of the $Cu_{47.5}Zr_{47.5}Al_5$ alloy showing a glass transition at 698 K followed by crystallization.

Table 1
Elastic constants (elastic modulus E, Poisson's ratio ν, shear modulus μ, and bulk modulus B) and thermal properties determined at 40 K/min heating rate (glass transition temperature T_g, onset of the crystallization temperature T_x, and extension of the supercooled liquid region ΔT_x) of the investigated BMGs

Composition	E (GPa)	μ (GPa)	B (GPa)	ν	T_g (K)	T_x (K)	ΔT_x (K)
$Cu_{50}Zr_{50}$	85.0	31.3	101.2	0.350	671	717	46
$Cu_{47.5}Zr_{47.5}Al_5$	88.7	33.0	113.7	0.365	698	772	74

condition. However, the length of the deformed/fractured specimen was also measured with the help of a micrometer screw gauge, which was observed to well fit with data obtained from the displacement of the machine cross heads. In addition, the elastic constants were calculated from ultrasonic sound velocity measurements.

The fracture surface and the specimen surface features after failure were investigated using a standard scanning electron microscope (SEM, Zeiss DSM 962) as well as a high resolution scanning electron microscope (Philips XL 30 operated with a field emission gun at 12 kV) to reveal the deformation and fracture characteristics of the alloys.

3. Results and discussion

The X-ray diffraction patterns of the investigated $Cu_{50}Zr_{50}$ and $Cu_{47.5}Zr_{47.5}Al_5$ alloys are presented in Fig. 1. Both as-cast alloys show broad diffraction maxima characteristic for an amorphous structure. The DSC traces of both alloys display a glass transition prior to crystallization during constant-rate heating at 40 K/min. A typical DSC trace for the $Cu_{47.5}Zr_{47.5}Al_5$ alloy is shown in Fig. 2. The glass transition temperatures of the alloys (defined as the onset temperature of the endothermic DSC event) are 671 K for $Cu_{50}Zr_{50}$ and 698 K for $Cu_{47.5}Zr_{47.5}Al_5$, respectively. The onset temperature of crystallization T_x of $Cu_{47.5}Zr_{47.5}Al_5$ is higher (698 K) than the value measured for $Cu_{50}Zr_{50}$ (671 K). Apparently, the addition of 5 at.% Al shifts the crystallization to higher temperatures and increases the width of the supercooled liquid region ($\Delta T = T_x - T_g$) from 46 to 76 K (Table 1). Altogether, the thermal stability data indicate an increased thermal stability of the ternary alloy compared to binary $Cu_{50}Zr_{50}$. This can be understood from thermodynamic considerations, since the heat of mixing of Cu–Zr pairs (-23 kJ/mole) is lower than that of Al–Zr pairs (-44 kJ/mole) [36] revealing the favorable effect of Al additions for enhancing the stability of the supercooled liquid.

Besides, the investigation of the glassy nature of the alloys through XRD and DSC experiments, TEM studies were performed to reveal the details of the structure at atomic resolution. Fig. 3 presents the high resolution TEM images for $Cu_{50}Zr_{50}$ and $Cu_{47.5}Zr_{47.5}Al_5$. The selected area electron diffraction (SAED) pattern from the $Cu_{50}Zr_{50}$ alloy reveals the presence of tiny crystallites in the glass, as shown in the inset in Fig. 3(a). The representative high resolution micrograph of this alloy displays lattice fringes of these tiny crystallites that can be clearly distinguished [marked by circles in Fig. 3(a)]. Their size is smaller than about 7 nm. The distribution of these crystallites is random and their volume fraction was estimated to be less than 10 vol.%. The high

resolution image of the amorphous structure of $Cu_{47.5}Zr_{47.5}Al_5$ is shown in Fig. 3(b). A representative microbeam SAED pattern of this alloy is given in the inset in Fig. 3(b). A weak contrast is overlapped on the bright amorphous ring in the SAED pattern indicating the presence of heterogeneities in the amorphous $Cu_{47.5}Zr_{47.5}Al_5$ phase. However, the exact heterogeneity in terms of short-range order, chemistry or undetectable crystallites could not be ascertained.

Fig. 4 shows the room temperature engineering stress–strain curves under compression. The $Cu_{50}Zr_{50}$ BMG exhibits an elastic strain (ε_y) of 1.7% and yields at $\sigma_y = 1272$ MPa. After yielding the stress increases with further deformation up to
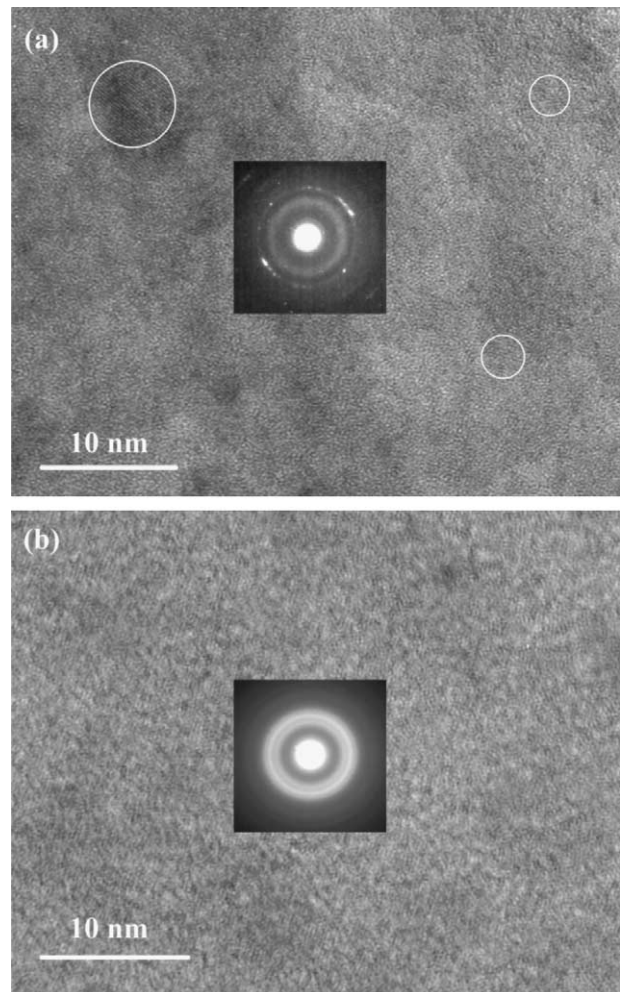

Fig. 3. TEM high resolution images of (a) $Zr_{50}Cu_{50}$, revealing tiny crystallites in the glassy matrix (marked by circles); inset: micro-beam diffraction pattern, corroborating the presence of nanocrystals in the glass; (b) Amorphous structure of $Cu_{47.5}Zr_{47.5}Al_5$; inset: the SAED pattern shows a weak contrast overlapping on the amorphous ring indicating an imhomogeneous glassy structure.
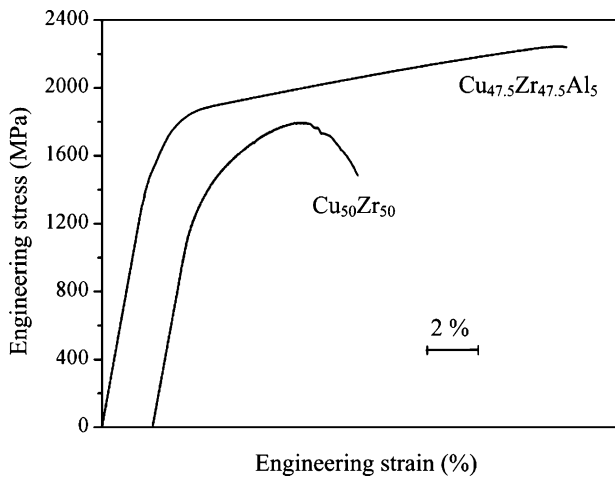
Fig. 4. Stress–strain curves of (a) $Cu_{50}Zr_{50}$, and (b) $Cu_{47.5}Zr_{47.5}Al_5$ under compression at a initial strain rate of $8 \times 10^{-4} \, s^{-1}$.

1794 MPa. The plastic strain (ε_p) was measured to be 4% in the case of $Cu_{50}Zr_{50}$, and then the stress decreases with further increasing strain and final failure occurs at $\varepsilon_f = 7.9\%$. The elastic modulus (E) was measured to be 84 GPa. On the other hand, the $Cu_{47.5}Zr_{47.5}Al_5$ BMG shows higher elastic strain ($\varepsilon_y = 2.0\%$) and yield strength ($\sigma_y = 1547$ MPa). Like the deformation behavior of $Cu_{50}Zr_{50}$, also the $Cu_{47.5}Zr_{47.5}Al_5$ BMG shows a stress increase after yielding and a large plastic strain ($\varepsilon_p = 16\%$). Failure occurs at 2265 MPa. Hence, the stress–strain curves of both alloys display a 'work hardening'-like behavior.

In addition to the compression tests, the elastic properties of the as-cast BMGs were estimated from ultrasonic sound velocity measurements. The obtained data are summarized in Table 1. The Poisson's ratio (ν), the shear modulus (μ) and the bulk modulus (B) calculated from the ultrasonic measurements are 0.35, 31.3, and 101.2 GPa for $Cu_{50}Zr_{50}$, and 0.365, 33.0, and 113.7 GPa for $Cu_{47.5}Zr_{47.5}Al_5$, respectively. The mechanism recently proposed to explain the enhanced ductility of BMGs [34] has emphasized the importance of a low value of the shear modulus (μ) and bulk modulus (B) ratio reflecting a high Poisson's ratio. This was supposed to enable shear collapse ahead of a shear band before crack nucleation. In the case of the present ductile Cu-base BMGs, the μ/B ratio is 0.309 and 0.290 for $Cu_{50}Zr_{50}$ and $Cu_{47.5}Zr_{47.5}Al_5$, respectively [35]. This value is significantly higher than the very low μ/B ratio of only 0.165 for the ductile Pt-base BMG [34], but close to the μ/B ratio of 0.31 reported for the well-known Vitreloy 1 bulk glass [34]. However, Vitreloy 1 exhibits rather brittle deformation behavior at room temperature. Therefore, a low μ/B ratio may not be the only reason for achieving ductilization of BMGs. Clearly, further more detailed investigations along this line are necessary to clarify this point.

The fractured specimens of both $Cu_{50}Zr_{50}$ and $Cu_{47.5}Zr_{47.5}Al_5$ BMGs show shear fracture, as depicted in Fig. 5. The macroscopic failure angle (θ_C^F) for $Cu_{50}Zr_{50}$ and $Cu_{47.5}Zr_{47.5}Al_5$ is measured to be 40.2 and 45°, respectively. The fracture surfaces of both the alloys exhibit vein-like patterns. A typical vein pattern of $Cu_{47.5}Zr_{47.5}Al_5$ is shown in Fig. 6(a). At higher magnification,

interactions of shear bands are observed under the veins in a few regions on the fracture surface [Fig. 6(b)]. Shear bands are also easily visible on the specimen surface. However, the number of visible shear bands at a particular magnification is lower in $Cu_{50}Zr_{50}$ than in the case of $Cu_{47.5}Zr_{47.5}Al_5$. Intersection of shear bands moving in primary direction (parallel to the final fracture plane) and secondary direction has been observed. The inter-shear band spacing is quite narrow, i.e. the shear bands are separated by a distance of about 1–2 μm in the case of $Cu_{50}Zr_{50}$. However, in the case of $Cu_{47.5}Zr_{47.5}Al_5$ the shear bands are highly branched and their movement is rather wavy in nature, as depicted in Fig. 6(c) (marked by dotted arrows). In this alloy the inter-shear band spacing is only about 150–500 nm, as observed by high resolution scanning electron microscopy. This confirms the formation of a high density of shear bands in this novel metallic glass.

The array of triangles in Fig. 6(c) indicates the passing of a set of parallel shear bands through another shear band moving into a different direction. The crossover over between the shear bands moving in different directions creates steps on each other and restricts their rapid propagation. This can further increase the stress level, as it observed during deformation (Fig. 4).
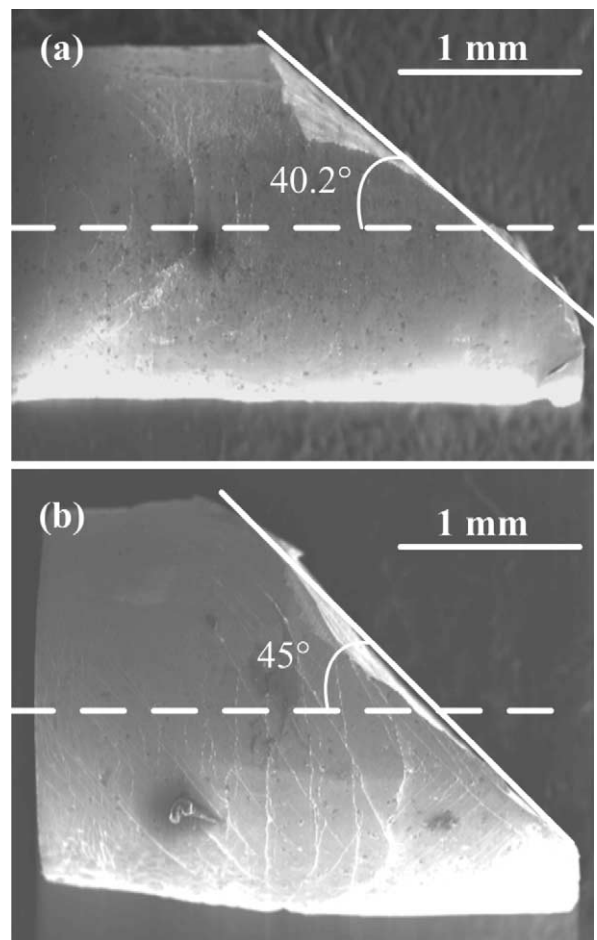

Fig. 5. SEM images of the deformed specimens: (a) $Cu_{50}Zr_{50}$ and (b) $Cu_{47.5}Zr_{47.5}Al_5$ showing significant barreling. This indicates a high flowability of the metallic glass at room temperature. The fracture angles of $Cu_{50}Zr_{50}$ and $Cu_{47.5}Zr_{47.5}Al_5$ are 40.2 and 45°, respectively.
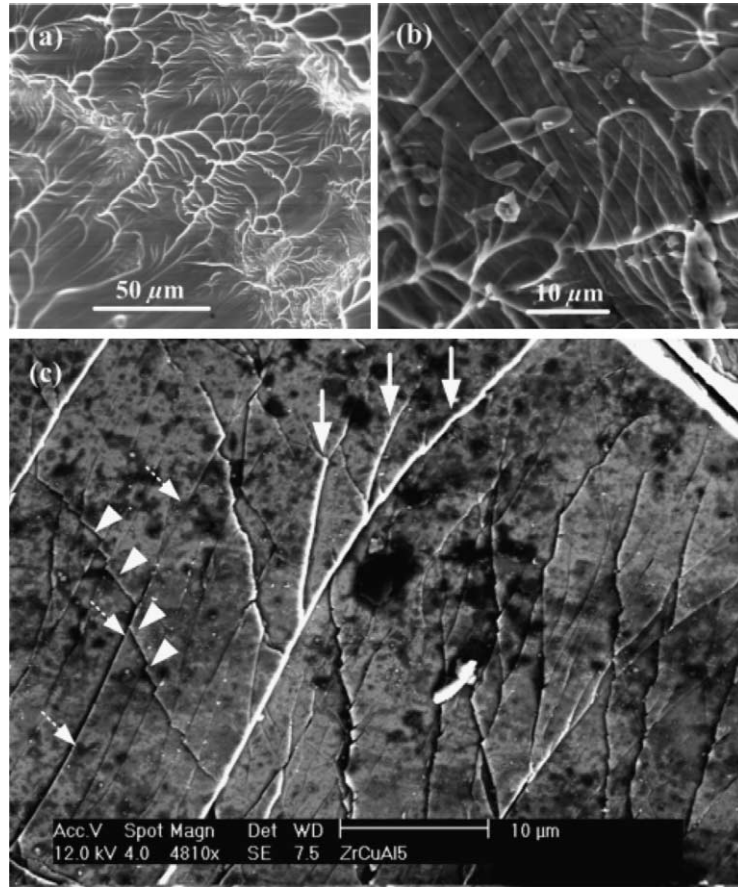
Fig. 6. SEM secondary electron images of a $Cu_{47.5}Zr_{47.5}Al_5$ specimen after failure: (a) vein pattern; (b) interaction of shear bands upon fracture; (c) strong branching (indicated by white arrows) and bending of shear bands (dotted arrows). The intersection of the shear bands gives a local locking effect and creates steps on the shear bands (marked by triangles) at the deformed specimen surface of $Cu_{47.5}Zr_{47.5}Al_5$ observed by high resolution scanning electron microscopy.

In this stage, the heterogeneous amorphous structure is believed to enable easy nucleation of shear bands at higher stress level due to primary and secondary shear band interactions and local restriction of shear band propagation. The increase in strain further enhances bending of the shear bands moving to both primary and secondary direction.

It is been reported [37] that the shear fracture mode of some nanostructured composites can be explained by a rotation mechanism of the shear bands due to a high compressive plasticity. In the present investigation, the plastic strain (ε_P) observed for the $Cu_{50}Zr_{50}$ and $Cu_{47.5}Zr_{47.5}Al_5$ BMGs is 4 and 16%, respectively. The final fracture angle (θ_C^F) measured for $Cu_{50}Zr_{50}$ and $Cu_{47.5}Zr_{47.5}Al_5$ is 40.2 and 45°, respectively. Therefore, the rotation mechanism of the shear bands can also be applied to these ductile Cu-base BMGs. In this model, a relationship between the initial shear band angle (θ_C^O), the final fracture angle after rotation (θ_C^F) and the plastic strain ε_p can be established by taking the rotation mechanism into account [37], i.e.

$$\sin(\theta_C^O) = \sqrt{1 - \varepsilon_P}\sin(\theta_C^F) \qquad (1)$$

From this relationship one can approximately estimate the initial shear band angle θ_C^O if the compressive plastic strain ε_P and the final measured shear fracture angle θ_C^F are known.

The initial shear band angles θ_C^O for the $Cu_{50}Zr_{50}$ and $Cu_{47.5}Zr_{47.5}Al_5$ BMGs are calculated to be 39.2 and 40.3°. Hence, these values are very close to $\sim 40°$ for both BMGs. This result agrees well with the previous observations for other BMGs and nanostructured composites [37] and follows the Mohr–Coulomb criterion [11,38,39]. It indicates that the multiplication of shear bands and their continuous interaction and intersection helps in rotating the shear direction showing a high compressive plasticity because of an obvious rotation of the initial shear bands.

The two investigated BMGs show differences in both structure and deformation behavior. In case of $Cu_{50}Zr_{50}$, very tiny randomly distributed nanocrystallites have been observed, which do not enhance the ductility significantly. However, the multiplication of shear bands and the distinct rotation of the shear plane results in a high plastic strain (16%), as observed for $Cu_{47.5}Zr_{47.5}Al_5$. Obviously, the addition of 5 at.% Al can suppress crystal nucleation during solidification under similar casting conditions (2 mm cross-section, cooling rate of 250 K/s) and enhances the glass-forming ability of the alloy [1]. The easy nucleation of shear bands is believed to be due to the intrinsic structural properties of the $Cu_{47.5}Zr_{47.5}Al_5$ glass, which promotes the nucleation of shear bands throughout the bulk material rather than triggering the nucleation of cracks. The intersection of shear bands (in three dimensions) decreases their

sharpness, hinders their rapid propagation and increases the flow stress of the material resulting a 'work hardening'-like behavior.

4. Conclusions

Novel Cu-based ductile bulk metallic glasses were prepared by slow cooling from the melt. This new class of metallic glass shows high strength up to 2265 MPa and high ductility up to 18% strain to failure. Besides, this $Cu_{47.5}Zr_{47.5}Al_5$ metallic glass shows a 'work hardening'-like behavior up to fracture. Addition of 5 at.% Al to the $Cu_{50}Zr_{50}$ glass increases the glass-forming ability, the thermal stability of the supercooled liquid as well as the yield strength (1547 MPa) of the material and improves its room temperature deformability even though the glass transition temperature (698 K) of the BMG is quite high. The intrinsic ductility is attributed to a heterogeneous amorphous structure, which enables easy and homogeneous nucleation of shear bands and their continuous multiplication during deformation. The interaction and intersection of the shear bands triggers their multiplication and increases the flowability of the BMG, thus increasing the flow stress of the material. The high compressive ductility of this class of metallic glass originates from dense shear band formation, shear band branching and shear band rotation from 40 to 45° along the shear plane during deformation.

Acknowledgements

References

[1] Tang MB, Zhao DQ, Pan MX, Wang WH. Chin Phys Lett 2004;2:901.
[2] Guo FQ, Poon SJ, Shiflet GJ. Appl Phys Lett 2004;84:37.
[3] Duan G, Xu D, Johnson WL. Metall Mater Trans 2005;36A:45.
[4] Inoue A, Zhang W, Zhang T, Kurosaka K. Acta Mater 2001;49:2645.
[5] Xu DH, Lohwongwatana B, Duan G, Johnson WL, Garland C. Acta Mater 2004;52:2621.
[6] Inoue A, Wang W. Mater Trans 2002;43:2921.
[7] Xu D, Duan G, Johnson WL. Phys Rev Lett 2004;92:245504.
[8] Greer AL. Science 1995;267:1947.
[9] Spaepen F. Acta Metall 1977;25:42.
[10] Chen H, He Y, Shiflet GJ, Poon SJ. Nature 1994;367:541.
[11] Zhang ZF, He G, Eckert J, Schultz L. Phys Rev Lett 2003;91:045505.
[12] Leonhard A, Xing LQ, Heilmaier M, Gebert A, Eckert J, Schultz L. Nanostruct Mater 1998;10:805.
[13] Fan C, Takeuchi A, Inoue A. Mater Trans JIM 1999;40:42.
[14] Xing LQ, Eckert J, Löser W, Schultz L. Appl Phys Lett 1999;74:664.
[15] Inoue A, Zhang T, Saida J, Matsushita M, Chen MW, Sakurai T. Mater Trans JIM 1999;40:1137.
[16] Eckert J, Mattern N, Zinkevitch M, Seidel M. Mater Trans JIM 1998;39:623.
[17] Choi-Yim H, Busch R, Köster U, Johnson WL. Acta Mater 1999;47:2455.
[18] Eckert J, Kübler A, Schultz L. J Appl Phys 1999;85:7112.
[19] Conner RD, Choi-Yim H, Johnson WL. J Mater Res 1999;14:3292.
[20] Dandliker RB, Conner RD, Johnson WL. J Mater Res 1998;13:2896.
[21] Kim CP, Busch R, Masuhr A, Choi-Yim H, Johnson WL. Appl Phys Lett 2001;79:1456.
[22] Conner RD, Dandliker RB, Johnson WL. Acta Mater 1998;46:6089.
[23] Choi-Yim H, Johnson WL. Appl Phys Lett 1997;71:3808.
[24] Fan C, Ott RT, Hufnagel TC. Appl Phys Lett 2002;81:1.
[25] Hirano T, Kato H, Matsuo A, Kawamura Y, Inoue A. Mater Trans JIM 2000;41:1454.
[26] Hays CC, Kim CP, Johnson WL. Phys Rev Lett 2000;84:2901.
[27] Kühn U, Eckert J, Mattern N, Schultz L. Appl Phys Lett 2002;80:2478.
[28] Das J, Löser W, Kühn U, Eckert J, Roy SK, Schultz L. Appl Phys Lett 2003;82:4690.
[29] Eckert J, He G, Das J, Löser W. Mater Trans JIM 2003;44:1999.
[30] Das J, Güth A, Klauß HJ, Mickel C, Löser W, Eckert J, et al. Scripta Mater 2003;49:1189.
[31] He G, Eckert J, Löser W, Schultz L. Nat Mater 2003;2:33.
[32] He G, Löser W, Eckert J. Acta Mater 2003;51:5223.
[33] Xing LQ, Li Y, Ramesh KT, Li J, Hufnagel TC. Phys Rev B 2001;64:180201.
[34] Schroers J, Johnson WL. Phys Rev Lett 2004;93:255506.
[35] Das J, Tang MB, Kim KB, Theissmann R, Baier F, Wang WH, Eckert J. Phys Rev Lett; 2005;94:205501.
[36] Boer FR, Boom R, Matterns WCM, Miedema AR, Niessen AK. Cohesion in metals. Amsterdam: North-Holland; 1988.
[37] Zhang ZF, He G, Zhang H, Eckert J. Scripta Mater 2005;52:945.
[38] Donovan PE. Acta Metall 1989;37:445.
[39] Zhang ZF, Eckert J. Phys Rev Lett 2005;94:094301.